

# Exceptional compound plasmon-polariton waves

Akhlesh Lakhtakia

*NanoMM — Nanoengineered Metamaterials Group  
Department of Engineering Science and Mechanics  
Pennsylvania State University, University Park, PA 16802–6812, USA*

Chenzhang Zhou

*NanoMM — Nanoengineered Metamaterials Group  
Department of Engineering Science and Mechanics  
Pennsylvania State University, University Park, PA 16802–6812, USA*

Tom G. Mackay\*

*School of Mathematics and Maxwell Institute for Mathematical Sciences  
University of Edinburgh, Edinburgh EH9 3FD, UK  
and  
NanoMM — Nanoengineered Metamaterials Group  
Department of Engineering Science and Mechanics  
Pennsylvania State University, University Park, PA 16802–6812, USA*

## Abstract

Ordinarily, a trimaterial structure comprising a sufficiently thin metal film interposed between two homogeneous dielectric materials guides compound plasmon-polariton (CPP) waves, for which the fields on both sides of the metal film decay exponentially with distance from the nearest metal/dielectric interface. However, if one of the dielectric materials is anisotropic then the trimaterial structure can guide an exceptional CPP wave for a particular propagation direction. On the side of the metal film occupied by the anisotropic dielectric material, the fields of the exceptional CPP wave decay as the product of a linear function and an exponential function of the distance from the nearest metal/dielectric interface. The canonical boundary-value problem for CPP-wave propagation has been analyzed and solved numerically; thereby, the spatial field profiles for exceptional CPP waves for a uniaxial-dielectric/metal/isotropic-dielectric structure have been established.

## 1 Introduction

The planar interface of a homogeneous metal and a homogeneous dielectric material (even air) can guide surface-plasmon-polariton (SPP) waves at a frequency at which the real parts of the relative permittivities of the two partnering materials differ in sign [1]. In the canonical treatment of the boundary-value problem, each partnering material occupies a half space. The electromagnetic fields of an SPP wave drop off exponentially with distance from the interface. Since the skin depth [2] of a metal is very small, the metallic half space can be replaced by a sufficiently thick metal film [3, 4]. This replacement — which creates a dielectric/metal/dielectric trimaterial structure — allows the exploitation of SPP waves for optical sensing [5], communication [6, 7], and microscopy [8, 9].

---

\*E-mail: T.Mackay@ed.ac.uk.

Since a metal film has two faces, the waveguiding phenomenon is not as straightforward as that due to a single metal/dielectric interface [6, 10, 11]. If the metal film is sufficiently thick, the two metal/dielectric interfaces will not interact and each could guide an SPP wave all by itself. But, when the metal film is thin, the two metal/dielectric interfaces will interact to engender compound plasmon-polariton (CPP) waves.

The spatial profile of the electric and magnetic fields of a CPP wave depends on the constitutive properties of both dielectric materials as well as the metal which is assumed to be isotropic. The fields on either side of the metal film obey the  $4 \times 4$ -matrix ordinary differential equation [12, 13]

$$\frac{d}{dz}[\underline{f}(z)] = i[\underline{P}] \cdot [\underline{f}(z)], \quad (1)$$

where  $[\underline{f}(z)]$  is column 4-vector,  $[\underline{P}]$  is a  $4 \times 4$  matrix,  $i = \sqrt{-1}$ , and the  $z$  axis is aligned normal to the metal film. If the dielectric material on a specific side of the metal film is isotropic, then the fields of the CPP wave on that side decay exponentially with distance  $|z|$  from the metal film. This is because the matrix  $[\underline{P}]$  for the dielectric material on that side of the metal film is semisimply degenerate [14], i.e., it has two distinct eigenvalues, each with algebraic multiplicity equal to two and geometric multiplicity also equal to two.

If the dielectric material on a specific side of the metal film is anisotropic, then two possibilities arise as follows [14]:

- I. The matrix  $[\underline{P}]$  for the dielectric material on that side of the metal film is non-degenerate, i.e., it has four distinct eigenvalues, each with algebraic multiplicity equal to one and geometric multiplicity also equal to one. Then, the fields on that side decay exponentially with distance  $|z|$  from the metal film [15].
- II. The matrix  $[\underline{P}]$  for the dielectric material on that side of the metal film is non-semisimply degenerate, i.e., it has two distinct eigenvalues, each with algebraic multiplicity equal to two but geometric multiplicity equal to one. Then, the fields on that side vary as the products of a linear function and an exponential function of the distance  $|z|$  from the metal film [16], decaying as  $|z| \rightarrow \infty$  [15].

Case I is commonplace, but this paper introduces Case II for CPP-wave propagation guided by a metal film interposed between two homogeneous dielectric materials. As non-semisimple degeneracy cannot be exhibited by an isotropic dielectric material, at least one of the two dielectric materials must be anisotropic. There are no other restrictions on that anisotropic material: it can be dissipative, active, or neither dissipative nor active.

In this paper, we consider CPP-wave propagation when one of the two dielectric materials (labeled  $\mathcal{A}$ ) is uniaxial with its optic axis aligned normal to the thickness direction of the metal film and the other dielectric material (labeled  $\mathcal{C}$ ) is isotropic, the two being separated by a film of a metal (labeled  $\mathcal{B}$ ). The matrixes  $[\underline{P}_{\mathcal{B}}]$  and  $[\underline{P}_{\mathcal{C}}]$  for materials  $\mathcal{B}$  and  $\mathcal{C}$ , respectively, are semisimply degenerate. When the matrix  $[\underline{P}_{\mathcal{A}}]$  is non-semisimply degenerate, the CPP wave may be classified as *exceptional*, following the terminology used first in condensed-matter physics [17, 18] and now increasingly in classical electromagnetics [16, 19–21]. When the matrix  $[\underline{P}_{\mathcal{A}}]$  is either non-degenerate or semisimply degenerate, the CPP wave is *unexceptional*.

Theory is presented in Sec. 2 and illustrative numerical results are provided and discussed in Sec. 3. The paper closes with some remarks in Sec. 4. Throughout the paper, the free-space permittivity, permeability, wavenumber, wavelength, and impedance are written as  $\varepsilon_0$ ,  $\mu_0$ ,  $k_0 = \omega\sqrt{\varepsilon_0\mu_0}$ ,  $\lambda_0 = 2\pi/k_0$ , and  $\eta_0 = \sqrt{\mu_0/\varepsilon_0}$ , respectively, with  $\omega$  being the angular frequency. Single underlining with no enclosing square brackets signifies a 3-vector. The position vector is denoted by  $\underline{r} = x\underline{\hat{u}}_x + y\underline{\hat{u}}_y + z\underline{\hat{u}}_z$ , where  $\{\underline{\hat{u}}_x, \underline{\hat{u}}_y, \underline{\hat{u}}_z\}$  is the triad of unit vectors aligned with the Cartesian axes. Double underlining with no enclosing square brackets signifies a  $3 \times 3$  dyadic [22]. Matrixes and column vectors are double and single underlined, respectively, and enclosed by square brackets. The superscript  $T$  denotes the transpose. The operators  $\text{Re}\{\cdot\}$  and  $\text{Im}\{\cdot\}$  deliver the real and imaginary parts, respectively, of complex-valued quantities; the complex conjugate is denoted by an asterisk; and dependence on time  $t$  is achieved implicitly through  $\exp(-i\omega t)$ .

## 2 Theory

### 2.1 4×4 matrix ordinary-differential-equation formalism

The dielectric material  $\mathcal{A}$  fills the half-space  $z > D$ , the dielectric material  $\mathcal{C}$  fills the half-space  $z < 0$ , the two being separated by the metal  $\mathcal{B}$  in the region  $0 < z < D$ , as shown in Fig. 1.

Material  $\mathcal{A}$  is uniaxial dielectric specified by the relative permittivity dyadic [22]

$$\underline{\underline{\epsilon}}_{\mathcal{A}} = \epsilon_{\mathcal{A}}^s \underline{\underline{I}} + (\epsilon_{\mathcal{A}}^t - \epsilon_{\mathcal{A}}^s) \hat{u}_x \hat{u}_x, \quad (2)$$

with  $\epsilon_{\mathcal{A}}^s \in \mathbb{C}$  and  $\epsilon_{\mathcal{A}}^t \in \mathbb{C}$  being the principal relative permittivity scalars and  $\underline{\underline{I}}$  being the identity 3×3 dyadic. We set  $\text{Re}\{\epsilon_{\mathcal{A}}^s\} > 1$ ,  $\text{Re}\{\epsilon_{\mathcal{A}}^t\} > 1$ ,  $\text{Im}\{\epsilon_{\mathcal{A}}^s\} \geq 0$ , and  $\text{Im}\{\epsilon_{\mathcal{A}}^t\} \geq 0$ . The intermediate material  $\mathcal{B}$  is a metal with relative permittivity  $\epsilon_{\mathcal{B}} \in \mathbb{C}$  such that  $\text{Re}\{\epsilon_{\mathcal{B}}\} < 0$  and  $\text{Im}\{\epsilon_{\mathcal{B}}\} > 0$ . Finally, the dielectric material  $\mathcal{C}$  is isotropic and is characterized by the relative permittivity  $\epsilon_{\mathcal{C}} \in \mathbb{C}$  with  $\text{Re}\{\epsilon_{\mathcal{C}}\} > 1$  and  $\text{Im}\{\epsilon_{\mathcal{C}}\} \geq 0$ .

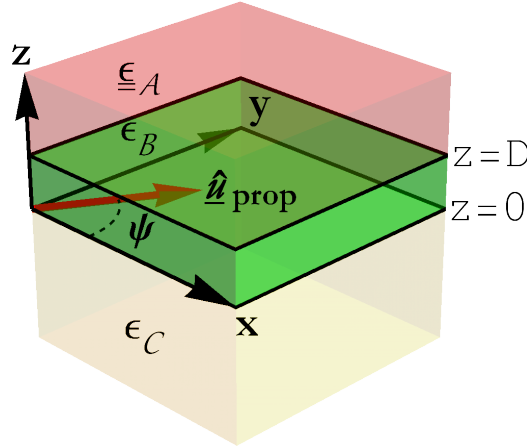


Figure 1: Schematic of the canonical boundary-value problem for the propagation of CPP waves parallel to the unit vector  $\hat{u}_{\text{prop}}$  that lies wholly in the  $xy$  plane at an angle  $\psi$  relative to the  $x$  axis.

The electric and magnetic field phasors for CPP-wave propagation are expressed everywhere as [15]

$$\left. \begin{aligned} \underline{E}(\underline{r}) &= [e_x(z) \hat{u}_x + e_y(z) \hat{u}_y + e_z(z) \hat{u}_z] \exp(iq \hat{u}_{\text{prop}} \cdot \underline{r}) \\ \underline{H}(\underline{r}) &= [h_x(z) \hat{u}_x + h_y(z) \hat{u}_y + h_z(z) \hat{u}_z] \exp(iq \hat{u}_{\text{prop}} \cdot \underline{r}) \end{aligned} \right\}, \quad z \in (-\infty, \infty), \quad (3)$$

with  $q$  being the guide wavenumber. Relative to the  $x$  axis, the direction of propagation in the  $xy$  plane is identified by the unit vector

$$\hat{u}_{\text{prop}} = \hat{u}_x \cos \psi + \hat{u}_y \sin \psi, \quad (4)$$

where the angle  $\psi \in [0, 2\pi)$ . Substitution of the phasor representations (3) in the source-free Maxwell curl equations yields the 4×4 matrix ordinary differential equations [12, 13]

$$\frac{d}{dz} [\underline{f}(z)] = \begin{cases} i[\underline{P}_{\mathcal{A}}] \cdot [\underline{f}(z)], & z > D \\ i[\underline{P}_{\mathcal{B}}] \cdot [\underline{f}(z)], & 0 < z < D \\ i[\underline{P}_{\mathcal{C}}] \cdot [\underline{f}(z)], & z < 0 \end{cases}, \quad (5)$$

wherein the column 4-vector

$$[\underline{f}(z)] = [ e_x(z), e_y(z), h_x(z), h_y(z) ]^T, \quad (6)$$

and the 4×4 propagation matrixes [23]

$$[\underline{P}_{\mathcal{A}}] = \begin{bmatrix} 0 & 0 & \frac{q^2 \cos \psi \sin \psi}{\omega \varepsilon_0 \varepsilon_{\mathcal{A}}^s} & \frac{k_0^2 \varepsilon_{\mathcal{A}}^s - q^2 \cos^2 \psi}{\omega \varepsilon_0 \varepsilon_{\mathcal{A}}^s} \\ 0 & 0 & \frac{-k_0^2 \varepsilon_{\mathcal{A}}^s + q^2 \sin^2 \psi}{\omega \varepsilon_0 \varepsilon_{\mathcal{A}}^s} & \frac{-q^2 \cos \psi \sin \psi}{\omega \varepsilon_0 \varepsilon_{\mathcal{A}}^s} \\ -\frac{q^2 \cos \psi \sin \psi}{\omega \mu_0} & \frac{-k_0^2 \varepsilon_{\mathcal{A}}^s + q^2 \cos^2 \psi}{\omega \mu_0} & 0 & 0 \\ \frac{k_0^2 \varepsilon_{\mathcal{A}}^t - q^2 \sin^2 \psi}{\omega \mu_0} & \frac{q^2 \cos \psi \sin \psi}{\omega \mu_0} & 0 & 0 \end{bmatrix} \quad (7)$$

and

$$[\underline{P}_{\ell}] = \begin{bmatrix} 0 & 0 & \frac{q^2 \cos \psi \sin \psi}{\omega \varepsilon_0 \varepsilon_{\ell}} & \frac{k_0^2 \varepsilon_{\ell} - q^2 \cos^2 \psi}{\omega \varepsilon_0 \varepsilon_{\ell}} \\ 0 & 0 & \frac{-k_0^2 \varepsilon_{\ell} + q^2 \sin^2 \psi}{\omega \varepsilon_0 \varepsilon_{\ell}} & \frac{-q^2 \cos \psi \sin \psi}{\omega \varepsilon_0 \varepsilon_{\ell}} \\ -\frac{q^2 \cos \psi \sin \psi}{\omega \mu_0} & \frac{-k_0^2 \varepsilon_{\ell} + q^2 \cos^2 \psi}{\omega \mu_0} & 0 & 0 \\ \frac{k_0^2 \varepsilon_{\ell} - q^2 \sin^2 \psi}{\omega \mu_0} & \frac{q^2 \cos \psi \sin \psi}{\omega \mu_0} & 0 & 0 \end{bmatrix}, \quad \ell \in \{\mathcal{B}, \mathcal{C}\}. \quad (8)$$

Whereas

$$h_z(z) = \frac{q [e_y(z) \cos \psi - e_x(z) \sin \psi]}{\omega \mu_0}, \quad z \in (-\infty, \infty), \quad (9)$$

holds in all three regions,

$$e_z(z) = \begin{cases} -\frac{q [h_y(z) \cos \psi - h_x(z) \sin \psi]}{\omega \varepsilon_0 \varepsilon_{\mathcal{A}}^s}, & z > D, \\ -\frac{q [h_y(z) \cos \psi - h_x(z) \sin \psi]}{\omega \varepsilon_0 \varepsilon_{\mathcal{B}}}, & 0 < z < D, \\ -\frac{q [h_y(z) \cos \psi - h_x(z) \sin \psi]}{\omega \varepsilon_0 \varepsilon_{\mathcal{C}}}, & z < 0. \end{cases} \quad (10)$$

## 2.2 Fields in material $\mathcal{A}$

The four eigenvalues of  $[\underline{P}_{\mathcal{A}}]$  can be written as  $\pm \alpha_{\mathcal{A}1}$  and  $\pm \alpha_{\mathcal{A}2}$ . The two with positive imaginary parts are

$$\left. \begin{aligned} \alpha_{\mathcal{A}1} &= i \sqrt{q^2 - k_0^2 \varepsilon_{\mathcal{A}}^s} \\ \alpha_{\mathcal{A}2} &= i \sqrt{\frac{q^2 [(\varepsilon_{\mathcal{A}}^s + \varepsilon_{\mathcal{A}}^t) - (\varepsilon_{\mathcal{A}}^s - \varepsilon_{\mathcal{A}}^t) \cos 2\psi] - 2k_0^2 \varepsilon_{\mathcal{A}}^s \varepsilon_{\mathcal{A}}^t}{2\varepsilon_{\mathcal{A}}^s}} \end{aligned} \right\}, \quad (11)$$

When  $\alpha_{\mathcal{A}1} \neq \alpha_{\mathcal{A}2}$ , the column vectors

$$[\underline{v}_{\mathcal{A}1}] = \begin{bmatrix} 0 \\ \frac{k_0 \alpha_{\mathcal{A}1}}{q^2 \sin \psi \cos \psi} \\ \frac{\cot 2\psi}{\eta_0} + \frac{\csc 2\psi}{\eta_0} \left( 1 - \frac{2k_0^2 \varepsilon_{\mathcal{A}}^s}{q^2} \right) \\ \eta_0^{-1} \end{bmatrix} \quad (12)$$

and

$$[\underline{v}_{\mathcal{A}2}] = \begin{bmatrix} 1 - \frac{q^2 (\cos 2\psi + 1)}{2k_0^2 \varepsilon_{\mathcal{A}}^s} \\ -\frac{q^2 \cos \psi \sin \psi}{k_0^2 \varepsilon_{\mathcal{A}}^s} \\ 0 \\ \frac{\alpha_{\mathcal{A}2}}{\omega \mu_0} \end{bmatrix} \quad (13)$$

are the eigenvectors of  $[\underline{P}_{\mathcal{A}}]$  matching the eigenvalues  $+\alpha_{\mathcal{A}1}$  and  $+\alpha_{\mathcal{A}2}$ , respectively, Hence, the general solution to Eq. (5)<sub>1</sub> is given as [15]

$$[\underline{f}(z)] = C_{\mathcal{A}1} [\underline{v}_{\mathcal{A}1}] \exp[i\alpha_{\mathcal{A}1}(z - D)] + C_{\mathcal{A}2} [\underline{v}_{\mathcal{A}2}] \exp[i\alpha_{\mathcal{A}2}(z - D)], \quad z > D, \quad (14)$$

for fields that decay as  $z \rightarrow +\infty$ . The complex-valued constants  $C_{\mathcal{A}1}$  and  $C_{\mathcal{A}2}$  have to be determined by application of appropriate boundary conditions at the plane  $z = D$ .

When  $[\underline{P}_{\mathcal{A}}]$  exhibits non-semisimple degeneracy,

$$\alpha_{\mathcal{A}1} = \alpha_{\mathcal{A}2} \equiv \alpha_{\mathcal{A}} = iq \sin \psi \quad (15)$$

and

$$q = \text{sgn}(\cos \psi) \frac{k_0 \sqrt{\varepsilon_{\mathcal{A}}^s}}{\cos \psi}, \quad (16)$$

where  $\text{sgn}(\zeta) = 1$  if  $\zeta > 0$  and  $\text{sgn}(\zeta) = -1$  if  $\zeta < 0$ . The square root in Eq. (16) must be chosen to ensure that  $\text{Im}\{\alpha_{\mathcal{A}}\} > 0$ . The general solution of Eq. (5)<sub>1</sub> is then expressed as [23]

$$[\underline{f}(z)] = (C_{\mathcal{A}1} [\underline{v}_{\mathcal{A}}] + k_0 C_{\mathcal{A}2} \{i(z - D) [\underline{v}_{\mathcal{A}}] + [\underline{w}_{\mathcal{A}}]\}) \exp[i\alpha_{\mathcal{A}}(z - D)], \quad z > D, \quad (17)$$

for fields that decay as  $z \rightarrow +\infty$ , where

$$[\underline{v}_{\mathcal{A}}] = \begin{bmatrix} 0 \\ \text{sgn}(\cos \psi) \frac{i}{\sqrt{\varepsilon_{\mathcal{A}}^s}} \\ 0 \\ \eta_0^{-1} \end{bmatrix} \quad (18)$$

and

$$[\underline{w}_A] = \frac{1}{k_0} \begin{bmatrix} \frac{2}{\varepsilon_A^t - \varepsilon_A^s} \\ \frac{\tan \psi}{\varepsilon_A^s} \left( \cot^2 \psi - 2 \frac{\varepsilon_A^s - \varepsilon_A^t \cot^2 \psi}{\varepsilon_A^s - \varepsilon_A^t} \right) \\ \operatorname{sgn}(\cos \psi) \frac{2i\sqrt{\varepsilon_A^s}}{\eta_0 (\varepsilon_A^t - \varepsilon_A^s)} \\ 0 \end{bmatrix}. \quad (19)$$

### 2.3 Fields in material $\mathcal{B}$

The  $4 \times 4$  matrix  $[\underline{P}_B]$  cannot exhibit non-semisimple degeneracy, and the general solution of Eq. (5)<sub>2</sub> can be stated as [13]

$$[\underline{f}(z)] = \exp \left\{ i[\underline{P}_B]z \right\} \cdot [\underline{f}(0^+)], \quad 0 < z < D, \quad (20)$$

which yields

$$[\underline{f}(D^-)] = \exp \left\{ i[\underline{P}_B]D \right\} \cdot [\underline{f}(0^+)]. \quad (21)$$

### 2.4 Fields in material $\mathcal{C}$

The  $4 \times 4$  matrix  $[\underline{P}_C]$  has two distinct eigenvalues  $\pm \alpha_C$ , where

$$\alpha_C = -i\sqrt{q^2 - k_0^2 \varepsilon_C}. \quad (22)$$

The sign of the square root in Eq. (22) must be such that  $\operatorname{Im} \{ \alpha_C \} < 0$  for CPP-wave propagation. The two linearly independent eigenvectors of  $[\underline{P}_C]$  corresponding to the eigenvalue  $\alpha_C$  are given by

$$\left. \begin{aligned} [\underline{v}_{C1}] &= \left[ 1 - \frac{q^2 \cos^2 \psi}{k_0^2 \varepsilon_C}, \quad -\frac{q^2 \cos \psi \sin \psi}{k_0^2 \varepsilon_C}, \quad 0, \quad \frac{\alpha_C}{\omega \mu_0} \right]^T \\ [\underline{v}_{C2}] &= \left[ \frac{q^2 \cos \psi \sin \psi}{k_0^2 \varepsilon_C}, \quad \frac{q^2 \sin^2 \psi}{k_0^2 \varepsilon_C} - 1, \quad \frac{\alpha_C}{\omega \mu_0}, \quad 0 \right]^T \end{aligned} \right\}. \quad (23)$$

Hence,

$$[\underline{f}(z)] = \{ C_{C1}[\underline{v}_{C1}] + C_{C2}[\underline{v}_{C2}] \} \exp(i\alpha_C z), \quad z < 0, \quad (24)$$

is the general solution of Eq. (5)<sub>3</sub> for fields that decay as  $z \rightarrow -\infty$ , wherein the complex-valued constants  $C_{C1}$  and  $C_{C2}$  have to be determined by applying boundary conditions at the plane  $z = 0$ .

### 2.5 Boundary conditions

The tangential components of the electric and magnetic field phasors must be continuous across the interface planes  $z = 0$  and  $z = D$ ; i.e.,

$$[\underline{f}(0^+)] = [\underline{f}(0^-)] \quad (25)$$

and

$$[\underline{f}(D^+)] = [\underline{f}(D^-)]. \quad (26)$$

The use of Eq. (21) therefore yields [15]

$$[\underline{f}(D^+)] = \exp \left\{ i[\underline{P}_B]D \right\} \cdot [\underline{f}(0^-)], \quad (27)$$

where

$$[\underline{f}(0^-)] = C_{c1}[\underline{v}_{c1}] + C_{c2}[\underline{v}_{c2}] \quad (28)$$

by virtue of Eq. (24). Next, either

$$[\underline{f}(D^+)] = C_{A1}[\underline{v}_{A1}] + C_{A2}[\underline{v}_{A2}] \quad (29)$$

from Eq. (14) leading to

$$C_{A1}[\underline{v}_{A1}] + C_{A2}[\underline{v}_{A2}] = \exp\left\{i[\underline{P}_{\underline{B}}]D\right\} \cdot \{C_{c1}[\underline{v}_{c1}] + C_{c2}[\underline{v}_{c2}]\} \quad (30)$$

or

$$[\underline{f}(D^+)] = C_{A1}[\underline{v}_{A}] + k_0 C_{A2}[\underline{w}_{A}] \quad (31)$$

from Eq. (17) delivering

$$C_{A1}[\underline{v}_{A}] + k_0 C_{A2}[\underline{w}_{A}] = \exp\left\{i[\underline{P}_{\underline{B}}]D\right\} \cdot \{C_{c1}[\underline{v}_{c1}] + C_{c2}[\underline{v}_{c2}]\} . \quad (32)$$

Both Eq. (30) and Eq. (32) can be put in the form

$$[\underline{Y}] \cdot [C_{A1}, C_{A2}, C_{c1}, C_{c2}]^T = [0, 0, 0, 0]^T. \quad (33)$$

As the  $4 \times 4$  characteristic matrix  $[\underline{Y}]$  must be singular for CPP-wave propagation, the dispersion equation

$$|[\underline{Y}]| = 0 \quad (34)$$

emerges.

If  $\psi$  is replaced by  $-\psi$  or by  $\pi \pm \psi$  then the dispersion equation (34) is unchanged. Accordingly, in the following numerical investigation of unexceptional and exceptional CPP waves, attention is restricted to the quadrant  $0 \leq \psi \leq \pi/2$ .

### 3 Numerical results and discussion

All calculations were made for  $\lambda_0 = 633$  nm fixed. Silver was chosen as the metal so that  $\varepsilon_B = -16.07 + 0.44i$  [24]. As the skin depth of silver then is 25.11 nm [2], the thickness  $D$  was varied in the range (0, 80] nm. The constitutive parameters  $\varepsilon_A^s$ ,  $\varepsilon_A^t$ , and  $\varepsilon_C$  were varied to bring out diverse facets of the CPP waves under investigation. In particular, material  $\mathcal{A}$  was chosen to be an effectively homogeneous material comprising electrically small spheroidal inclusions distributed in a host material; by varying the volume fraction and elongation of the inclusions, as well as the permittivities of the inclusion and host materials, the constitutive parameters  $\varepsilon_A^s$  can be  $\varepsilon_A^t$  adjusted [27, 28]. In contrast, material  $\mathcal{C}$  was chosen to be a natural one. The angle  $\psi \in [0, \pi/2]$  to fix the direction of propagation was varied to find a value at which an exceptional CPP wave can exist.

Let us begin by choosing  $\varepsilon_A^s = 1.5 + 0.5i$ ,  $\varepsilon_A^t = 3.1282 + 0.1111i$ , and  $\varepsilon_C = 6.26$  (zinc selenide [29]). The solutions of Eq. (34) as functions of  $D \in (0, 80]$  nm for  $\psi = 25^\circ$  are organized into four branches in Fig. 2 as follows:

- I. The shortest branch commences at  $D = 0^+$  and terminates at  $D \simeq 0.83$  nm.
- II. The next longer branch commences at  $D = 0^+$  and terminates at  $D \simeq 3.43$  nm.
- III. The next longer branch begins at  $D \simeq 8.55$  nm. After  $D$  increases beyond 60 nm, the solution on this branch tends towards  $(1.3679 + 0.2251i)k_0$ , which is the wavenumber of the SPP wave guided solely by the  $\mathcal{A}/\mathcal{B}$  interface [30].

IV. The longest branch commences at  $D = 0^+$  and the solution on this branch tends towards  $q = (3.2012 + 0.0279i)k_0$  as  $D$  increases, which is the wavenumber of the SPP wave guided solely by the  $\mathcal{B}/\mathcal{C}$  interface [1, 15].

Both (i) the existence of Branches I and II as well as (ii) the deviation of Branches III and IV from their respective asymptotes indicate the interaction of the  $\mathcal{A}/\mathcal{B}$  and  $\mathcal{B}/\mathcal{C}$  interfaces in the creation of CPP waves that are not merely the spatial superpositions of the SPP waves guided either by the  $\mathcal{A}/\mathcal{B}$  interface by itself or the  $\mathcal{B}/\mathcal{C}$  interface by itself.

Hence, CPP waves can be said to exist for  $D > 0$ . These are of the unexceptional kind, except that the CPP wave on Branch III for  $D = 60$  nm is exceptional because  $[\underline{P}_{\mathcal{A}}]$  exhibits a non-semisimple degeneracy. The fact that the exceptional CPP wave exists on Branch III alone was unsurprising in retrospect, because the solution on this branch tends towards  $q \simeq (1.3679 + 0.2251i)k_0$  and the  $\mathcal{A}/\mathcal{B}$  interface by itself can support the existence of an exceptional SPP wave with  $q = (1.3695 + 0.2222i)k_0$  [30].

The surface wave guided by the interface of materials  $\mathcal{A}$  and  $\mathcal{C}$  when  $D = 0$  is classified as a Dyakonov surface wave [15, 25, 26]. The wavenumbers of the two Dyakonov surface waves guided by the  $\mathcal{A}/\mathcal{C}$  interface by itself are  $q = (1.2095 + 0.1862i)k_0$  and  $q = (0.9642 + 0.1556i)k_0$  [31, 32]. Thus, both Branches I and II of unexceptional CPP waves can be extended to include the Dyakonov surface waves that exist for  $D = 0$ .

Both  $\text{Re}\{q\}$  and  $\text{Im}\{q\}$  on Branch IV rise monotonically and rapidly as  $D \rightarrow 0^+$ . Thus, the phase speed  $\omega/\text{Re}\{q\}$  decreases and the attenuation rate  $\text{Im}\{q\}$  increases [15], and the unexceptional CPP wave becomes ineffective as a transporter of electromagnetic energy.

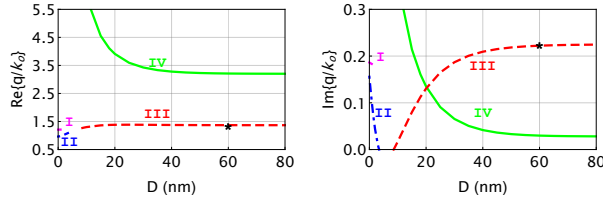


Figure 2:  $\text{Re}\{q/k_0\}$  and  $\text{Im}\{q/k_0\}$  plotted versus  $D \in (0, 80]$  nm for CPP waves when  $\varepsilon_{\mathcal{A}}^s = 1.5 + 0.5i$ ,  $\varepsilon_{\mathcal{A}}^t = 3.1282 + 0.1111i$ ,  $\varepsilon_{\mathcal{B}} = -16.07 + 0.44i$ ,  $\varepsilon_{\mathcal{C}} = 6.26$ ,  $\psi = 25^\circ$ , and  $\lambda_0 = 633$  nm. The solitary exceptional point of  $[\underline{P}_{\mathcal{A}}]$  is identified by a black star in both plots. The solution branches are numbered I to IV.

The matrix  $[\underline{P}_{\mathcal{A}}]$  exhibits non-semisimple degeneracy in Fig. 2 at a value of  $D$  that is more than twice the skin depth of silver, so that the exceptional CPP wave is almost an exceptional SPP wave guided by the  $\mathcal{A}/\mathcal{B}$  interface all by itself. In order for the exceptional CPP wave to occur at a smaller value of  $D$  so that the  $\mathcal{A}/\mathcal{B}$  and  $\mathcal{B}/\mathcal{C}$  interfaces interact, we changed the extraordinary relative permittivity scalar [22] of material  $\mathcal{A}$  to  $\varepsilon_{\mathcal{A}}^t = 1.6173 + 0.6659i$  and chose perfluorohexane ( $\text{C}_6\text{F}_{14}$ ) as material  $\mathcal{C}$  so that  $\varepsilon_{\mathcal{C}} = 1.5625$  [33]. All other parameters were left the same as for Fig. 2.

The solutions of Eq. (34) as functions of  $D \in (0, 80]$  nm are organized into two branches in Fig. 3 as follows:

- I. This branch starts at  $D = 0^+$ . Both  $\text{Re}\{q\}$  and  $\text{Im}\{q\}$  increase as  $D$  increases to  $\sim 20$  nm. As  $D$  increases further,  $\text{Re}\{q\}$  increases but  $\text{Im}\{q\}$  decreases and the solution on this branch tends towards  $(1.3155 + 0.0019i)k_0$ , which is the wavenumber of the SPP wave guided solely by the  $\mathcal{B}/\mathcal{C}$  interface [1, 15].
- II. This branch starts at  $D = 0^+$  with very large values of  $\text{Re}\{q\}$  and  $\text{Im}\{q\}$  so that the corresponding CPP wave is not an effective transporter of electromagnetic energy. However, both  $\text{Re}\{q\}$  and  $\text{Im}\{q\}$  decline rapidly and do not change significantly for  $D > 50$  nm. After  $D$  increases beyond 40 nm, the solution on this branch tends towards  $(1.3011 + 0.2422i)k_0$ , which is the wavenumber of the SPP wave guided solely by the  $\mathcal{A}/\mathcal{B}$  interface [30]. The matrix  $[\underline{P}_{\mathcal{A}}]$  exhibits a non-semisimple degeneracy at  $D = 30$  nm, giving rise to an exceptional CPP wave on Branch II with  $q = (1.3695 + 0.2222i)k_0$ .

The planar interface of materials  $\mathcal{A}$  and  $\mathcal{C}$  can guide a Dyakonov surface wave in the direction specified by  $\psi = 25^\circ$ . The wavenumber of this surface wave is  $q = (0.9364 + 0.0334i)k_0$ , which means that Branch I of unexceptional CPP waves can be extended to include the Dyakonov surface wave that exists for  $D = 0$ .

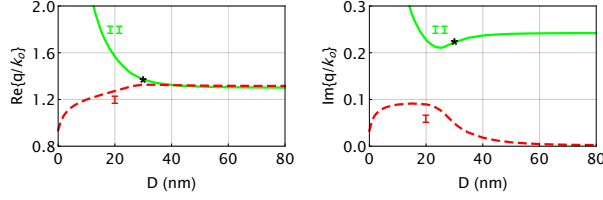


Figure 3:  $\text{Re}\{q/k_0\}$  and  $\text{Im}\{q/k_0\}$  plotted versus  $D \in (0, 80]$  nm for CPP waves when  $\varepsilon_{\mathcal{A}}^s = 1.5 + 0.5i$ ,  $\varepsilon_{\mathcal{A}}^t = 1.6173 + 0.6659i$ ,  $\varepsilon_{\mathcal{B}} = -16.07 + 0.44i$ ,  $\varepsilon_{\mathcal{C}} = 1.5625$ ,  $\psi = 25^\circ$ , and  $\lambda_0 = 633$  nm. The solitary exceptional point of  $[\underline{P}_{\mathcal{A}}]$  is identified by a black star in both plots. The solution branches are numbered I and II.

Finally, we modified the constitutive parameters to  $\varepsilon_{\mathcal{A}}^t = 1.7896 + 0.4807i$  and  $\varepsilon_{\mathcal{C}} = 1.6066$  and the direction of propagation to  $\psi = 23^\circ$ , in order to obtain an exceptional CPP wave and an unexceptional CPP wave with identical phase speeds for the same value of  $D$ . The solutions of Eq. (34) as functions of  $D \in (0, 80]$  nm are organized into two branches in Fig. 4 as follows:

- I. This branch starts at  $D = 0.58$  nm. Both  $\text{Re}\{q\}$  and  $\text{Im}\{q\}$  increase as  $D$  increases to  $\sim 20$  nm. As  $D$  increases further,  $\text{Re}\{q\}$  increases but  $\text{Im}\{q\}$  decreases and the solution on this branch tends towards  $(1.3360 + 0.0020i)k_0$ , which is the wavenumber of the SPP wave guided solely by the  $\mathcal{B}/\mathcal{C}$  interface [1, 15].
- II. This branch starts at  $D = 0^+$  with very large values of  $\text{Re}\{q\}$  and  $\text{Im}\{q\}$  so that the corresponding CPP wave is an ineffective transporter of electromagnetic energy. However, both  $\text{Re}\{q\}$  and  $\text{Im}\{q\}$  decline rapidly. After  $D$  increases beyond 40 nm, the solution on this branch tends towards  $(1.3089 + 0.2366i)k_0$ , which is the wavenumber of the SPP wave guided solely by the  $\mathcal{A}/\mathcal{B}$  interface [30].

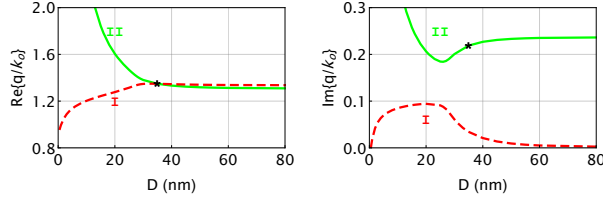


Figure 4:  $\text{Re}\{q/k_0\}$  and  $\text{Im}\{q/k_0\}$  plotted versus  $D \in (0, 80]$  nm for CPP waves when  $\varepsilon_{\mathcal{A}}^s = 1.5 + 0.5i$ ,  $\varepsilon_{\mathcal{A}}^t = 1.7896 + 0.4807i$ ,  $\varepsilon_{\mathcal{B}} = -16.07 + 0.44i$ ,  $\varepsilon_{\mathcal{C}} = 1.6066$ ,  $\psi = 23^\circ$ , and  $\lambda_0 = 633$  nm. The solitary exceptional point of  $[\underline{P}_{\mathcal{A}}]$  is identified by a black star in both plots. The solution branches are numbered I and II.

The matrix  $[\underline{P}_{\mathcal{A}}]$  exhibits non-semisimple degeneracy at  $D = 35$  nm, giving rise to an exceptional CPP wave on Branch II with  $q = (1.3484 + 0.2188i)k_0$ . For the same value of  $D$ , an unexceptional CPP wave exists on Branch I with  $q = (1.3484 + 0.0342i)k_0$ . Since  $\text{Re}\{q\}$  is the same for both CPP waves, they have the same phase speed. However, the exceptional CPP wave attenuates in the direction of propagation with a higher rate than the unexceptional CPP wave.

No Dyakonov surface wave can be guided by the planar interface of materials  $\mathcal{A}$  and  $\mathcal{B}$  when  $\psi = 23^\circ$ . Therefore, Branch I cannot be extended to  $D = 0$ .

Given that the unexceptional and the exceptional CPP waves at  $D = 35$  nm in Fig. 4 have the same phase speed, we decided to examine the spatial profiles of  $\underline{E}(r)$  and  $\underline{H}(r)$ , as well as of the time-averaged

Poynting vector

$$\underline{P}(\underline{r}) = \frac{1}{2} \text{Re} \{ \underline{E}(\underline{r}) \times \underline{H}^*(\underline{r}) \} \quad (35)$$

of both waves. The magnitudes of components of all three quantities parallel to the unit vectors  $\hat{\underline{u}}_{\text{prop}}$ ,  $\hat{\underline{u}}_s = -\hat{\underline{u}}_x \sin \psi + \hat{\underline{u}}_y \cos \psi$ , and  $\hat{\underline{u}}_z$  evaluated for  $\underline{r} = z\hat{\underline{u}}_z$  are plotted in Fig. 5 for the unexceptional CPP wave [ $q = (1.3484 + 0.0342i)k_0$ ], and in Fig. 6 for the exceptional CPP wave [ $q = (1.3484 + 0.2188i)k_0$ ].

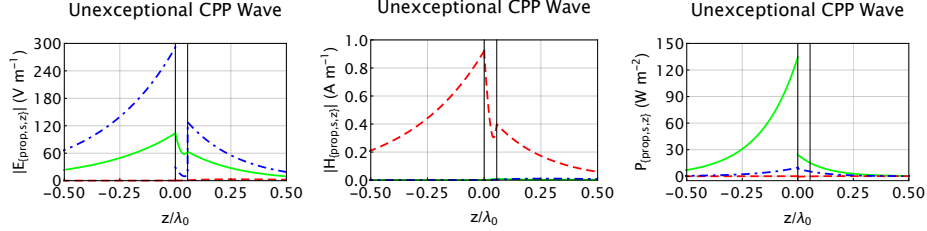


Figure 5:  $|\underline{E}(z\hat{\underline{u}}_z) \cdot \underline{n}|$ ,  $|\underline{H}(z\hat{\underline{u}}_z) \cdot \underline{n}|$ , and  $\underline{P}(z\hat{\underline{u}}_z) \cdot \underline{n}$  of the unexceptional CPP wave [ $q = (1.3484 + 0.0342i)k_0$ ] plotted versus  $z/\lambda_0$ , when  $\varepsilon_{\mathcal{A}}^s = 1.5 + 0.5i$ ,  $\varepsilon_{\mathcal{A}}^t = 1.7896 + 0.4807i$ ,  $\varepsilon_{\mathcal{B}} = -16.07 + 0.44i$ ,  $\varepsilon_{\mathcal{C}} = 1.6066$ ,  $\psi = 23^\circ$ ,  $D = 35$  nm, and  $\lambda_0 = 633$  nm. The normalization is such that  $|\underline{E}(D\hat{\underline{u}}_z) \cdot \hat{\underline{u}}_s| = 1$  V m<sup>-1</sup>. The left and right black vertical lines stand for the interfaces  $\mathcal{B}/\mathcal{C}$  and  $\mathcal{A}/\mathcal{B}$ , respectively. Key:  $\underline{n} = \hat{\underline{u}}_{\text{prop}}$  green solid curves;  $\underline{n} = \hat{\underline{u}}_s$  red dashed curves;  $\underline{n} = \hat{\underline{u}}_z$  blue broken-dashed curves.

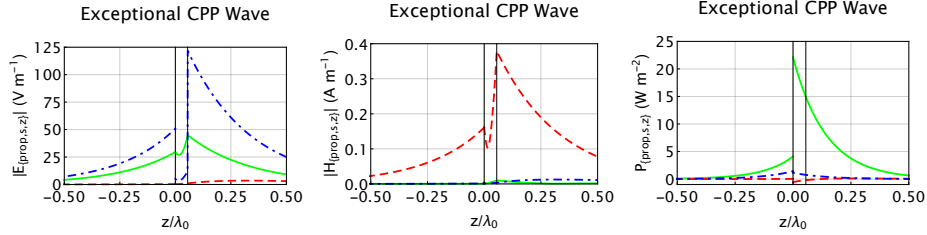


Figure 6: Same as Fig. 5 except for the exceptional CPP wave [ $q = (1.3484 + 0.2188i)k_0$ ].

The spatial profiles of the two CPP waves are very different from each other. The fields of the unexceptional CPP wave are higher in the isotropic material  $\mathcal{C}$  than in the anisotropic material  $\mathcal{A}$  and, therefore, a much larger fraction of the energy of the exceptional CPP wave is contained in material  $\mathcal{C}$  than in material  $\mathcal{A}$ . In contrast, the fields of the exceptional CPP wave are higher in the anisotropic material  $\mathcal{A}$  than in the isotropic material  $\mathcal{C}$  and, therefore, a much larger fraction of the energy of the exceptional CPP wave is contained in material  $\mathcal{A}$  than in material  $\mathcal{C}$ . Furthermore, given that  $|\underline{E}(D\hat{\underline{u}}_z) \cdot \hat{\underline{u}}_s| = 1$  V m<sup>-1</sup> in both figures, the maximum magnitudes of the Cartesian components of both fields and the time-averaged Poynting vector are higher for the exceptional CPP wave than for the unexceptional CPP wave.

Figures 7 and 8 provide a comparison of the spatial profiles of the electric fields of both types of CPP waves in the anisotropic material  $\mathcal{A}$ . This comparison is warranted by the fact that  $[\underline{P}_{\mathcal{A}}]$  is non-semisimply degenerate for the exceptional CPP wave but not for the unexceptional CPP wave, whereas  $[\underline{P}_{\mathcal{B}}]$  and  $[\underline{P}_{\mathcal{C}}]$  have the same eigenvalue characteristics for both types of CPP waves. Since  $\alpha_{\mathcal{A}1} \neq \alpha_{\mathcal{A}2}$  for the unexceptional CPP wave, the components of  $\underline{\Psi}(z) = \underline{E}(z\hat{\underline{u}}_z) \exp[-i\alpha_{\mathcal{A}1}(z - D)]$  vary with  $z$  in an undulating fashion in Fig. 7. On the other hand,  $\alpha_{\mathcal{A}1} = \alpha_{\mathcal{A}2}$  for the exceptional CPP wave, the components of  $\underline{\Psi}(z)$  vary linearly with  $z$  in Fig. 8. Parenthetically, the increase in the magnitudes of the plotted quantities with  $z$  in Fig. 8 should not cause alarm because attenuation as  $z \rightarrow \infty$  is due to  $\exp[-\text{Im}\{\alpha_{\mathcal{A}1}\}(z - D)]$ , but that has been factored out of the definition of  $\underline{\Psi}(z)$ .

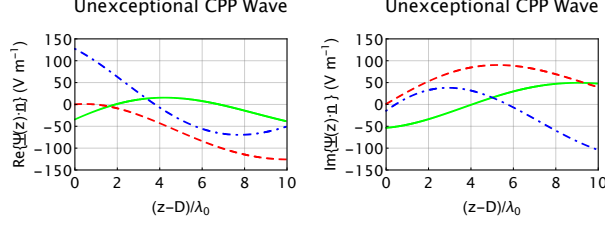


Figure 7:  $\text{Re}\{\underline{\Psi}(z) \cdot \underline{n}\}$  and  $\text{Im}\{\underline{\Psi}(z) \cdot \underline{n}\}$  of the unexceptional CPP wave [ $q = (1.3484 + 0.0342i)k_0$ ] plotted versus  $(z - D)/\lambda_0$ , when  $\varepsilon_{\mathcal{A}}^s = 1.5 + 0.5i$ ,  $\varepsilon_{\mathcal{A}}^t = 1.7896 + 0.4807i$ ,  $\varepsilon_{\mathcal{B}} = -16.07 + 0.44i$ ,  $\varepsilon_{\mathcal{C}} = 1.6066$ ,  $\psi = 23^\circ$ ,  $D = 35$  nm, and  $\lambda_0 = 633$  nm. The normalization is such that  $|\underline{E}(D\hat{u}_z) \cdot \hat{u}_s| = 1 \text{ V m}^{-1}$ . Key:  $\underline{n} = \hat{u}_{\text{prop}}$  green solid curves;  $\underline{n} = \hat{u}_s$  red dashed curves;  $\underline{n} = \hat{u}_z$  blue broken-dashed curves.

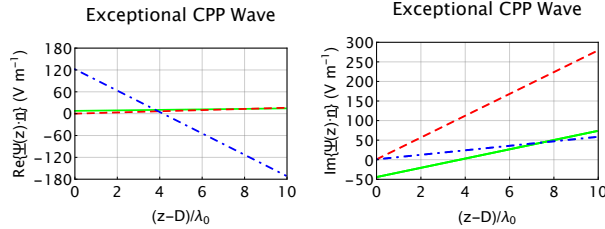


Figure 8: Same as Fig. 7 except for the exceptional CPP wave [ $q = (1.3484 + 0.2188i)k_0$ ].

## 4 Closing remarks

The objective of this paper is to introduce the concept of exceptional compound plasmon-polariton waves. Such waves are guided by a sufficiently thin metal film interposed between two homogeneous dielectric materials of which at least one must be anisotropic. Ordinarily, this arrangement will guide unexceptional CPP waves, i.e., the fields on either side of the metal film decay exponentially with distance from the nearest metal/dielectric interface. In contrast, the fields of an exceptional CPP wave decay on one side of the metal film as the product of a linear function and an exponential function of the distance from the nearest metal/dielectric interface.

The simplest scenario for exceptional CPP-wave propagation was considered in which one of the dielectric materials is uniaxial while the other is isotropic, and the metal is isotropic. Greater scope for exceptional CPP waves is likely to be presented by scenarios in which more than one of the materials in the trimaterial structure is anisotropic. In particular, if the one (or more) of the materials in a trimaterial structure is biaxial, then the prospect of multiple exceptional CPP waves arises [34]. These are matters for future investigation.

## Acknowledgements

A. L. thanks the Charles Godfrey Binder Endowment at Penn State for ongoing support of his research. This work was supported in part by EPSRC (grant number EP/S00033X/1).

## Disclosures

The authors declare that there are no conflicts of interest related to this article.

## References

- [1] J. M. Pitarke, V. M. Silkin, E. V. Chulkov, and P. M. Echenique, “Theory of surface plasmons and surface-plasmon polaritons,” <http://dx.doi.org/10.1088/0034-4885/70/1/R01> Rept. Prog. Phys. **70**, 1–87 (2007).
- [2] M. F. Iskander, *Electromagnetic Fields and Waves* (Waveland Press, 2013).
- [3] T. Turbadar, “Complete absorption of light by thin metal films,” <http://dx.doi.org/10.1088/0370-1328/73/1/307> Proc. Phys. Soc. **73**, 40–44 (1959).
- [4] T. Turbadar, “Complete absorption of plane polarized light by thin metal films,” <http://dx.doi.org/10.1080/713817875> Optica Acta **11**, 207–210 (1964).
- [5] J. Homola, ed., *Surface Plasmon Resonance Based Sensors* (Springer, 2006).
- [6] D. Sarid, “Long-range surface-plasma waves on very thin metal films,” <http://dx.doi.org/10.1103/PhysRevLett.47.1927> Phys. Rev. Lett. **47**, 1927–1930 (1981).
- [7] J. C. Quail, J. G. Rako, and H. J. Simon, “Long-range surface-plasmon modes in silver and aluminum films,” <http://dx.doi.org/10.1364/OL.8.000377> Opt. Lett. **8**, 377–379 (1983).
- [8] G. Stabler, M. G. Somekh, and C. W. See, “High-resolution wide-field surface plasmon microscopy,” <http://dx.doi.org/10.1111/j.0022-2720.2004.01309.x> J. Microsc. **214**, 328–333 (2004).
- [9] M. G. Somekh, “Surface plasmon and surface wave microscopy,” in *Optical Imaging and Microscopy*, P. Török and F.-J. Kao, eds. (Springer, 2007), pp. 347–399.
- [10] Y.-J. Jen, “Arbitrarily polarized long-range surface-plasmon-polariton waves,” <https://dx.doi.org/10.1117/1.3634056> J. Nanophoton. **5**, 050304 (2011).
- [11] Y. Akimov, “Optical resonances in Kretschmann and Otto configurations,” <https://doi.org/10.1364/OL.43.001195> Opt. Lett. **43**, 1195–1198 (2018).
- [12] D. W. Berreman, “Optics in stratified and anisotropic media: 4×4-matrix formulation,” <https://doi.org/10.1364/JOSA.62.000502> J. Opt. Soc. Am. **62**, 502–510 (1972).
- [13] T. G. Mackay and A. Lakhtakia, *The Transfer-Matrix Method in Electromagnetics and Optics* (Morgan & Claypool, 2020).
- [14] M. C. Pease III, *Methods of Matrix Algebra* (Academic, 1965).
- [15] J. A. Polo Jr., T. G. Mackay, and A. Lakhtakia, *Electromagnetic Surface Waves: A Modern Perspective* (Elsevier, 2013).
- [16] A. Lakhtakia and T. G. Mackay, “From unexceptional to doubly exceptional surface waves,” <https://doi.org/10.1364/JOSAB.399403> J. Opt. Soc. Am. B **37**, 2444–2451 (2020).
- [17] N. Moiseyev, *Non-Hermitian Quantum Mechanics* (Cambridge Univ., 2011).
- [18] K. Kawabata, T. Bessho, and M. Sato, “Classification of exceptional points and non-Hermitian topological semimetals,” <https://doi.org/10.1103/PhysRevLett.123.066405> Phys. Rev. Lett. **123**, 066405 (2019).
- [19] A. D. Kiselev and V. G. Chigrinov, “Optics of short-pitch deformed-helix ferroelectric liquid crystals: Symmetries, exceptional points, and polarization-resolved angular patterns,” <https://doi.org/10.1103/PhysRevE.90.042504> Phys. Rev. E **90**, 042504 (2014).

- [20] M. Grundmann, C. Sturm, C. Kranert, S. Richter, R. Schmidt-Grund, C. Deparis, and J. Zúñiga-Pérez, “Optically anisotropic media: New approaches to the dielectric function, singular axes, microcavity modes and Raman scattering intensities,” <https://doi.org/10.1002/pssr.201600295> Phys. Stat. Sol. RRL **11**, 1600295 (2017).
- [21] G. W. Hanson, A. B. Yakovlev, M. A. K. Othman, and F. Capolini, “Exceptional points of degeneracy and branch points for coupled transmission lines—Linear-algebra and bifurcation perspectives,” <https://doi.org/10.1109/TAP.2018.2879761> IEEE Trans. Antennas Propagat. **67**, 1025–1034 (2019).
- [22] H. C. Chen, *Theory of Electromagnetic Waves* (McGraw–Hill, 1983).
- [23] T. G. Mackay, C. Zhou, and A. Lakhtakia, “Dyakonov–Voigt surface waves,” <http://dx.doi.org/10.1098/rspa.2019.0317> Proc. R. Soc. Lond. A **475**, 20190317 (2019).
- [24] P. B. Johnson and R. W. Christy, “Optical constants of transition metals: Ti, V, Cr, Mn, Fe, Co, Ni, and Pd,” <http://dx.doi.org/10.1103/PhysRevB.9.5056> Phys. Rev. B **9**, 5056–5070 (1970).
- [25] F. N. Marchevskii, V. L. Strizhevskii, and S. V. Strizhevskii, “Singular electromagnetic waves in bounded anisotropic media,” Sov. Phys. Solid State **26**, 911–912 (1984).
- [26] M. I. D’yakonov, “New type of electromagnetic wave propagating at an interface,” Sov. Phys. JETP **67**, 714–716 (1988).
- [27] P. S. Neelakanta, *Handbook of Electromagnetic Materials* (CRC Press, 1995).
- [28] T. G. Mackay, “Effective constitutive parameters of linear nanocomposites in the long-wavelength regime,” <https://doi.org/10.1117/1.3626857> J. Nanophoton. **5**, 051001 (2011).
- [29] D. T. F. Marple, “Refractive index of ZnSe, ZnTe, and CdTe,” <https://doi.org/10.1063/1.1713411> J. Appl. Phys. **35**, 539–542 (1964).
- [30] C. Zhou, T. G. Mackay, and A. Lakhtakia, “Surface-plasmon-polariton wave propagation supported by anisotropic materials: Multiple modes and mixed exponential and linear localization characteristics,” <https://dx.doi.org/10.1103/PhysRevA.100.033809> Phys. Rev. A **100**, 033809 (2019).
- [31] C. J. Zapata-Rodríguez, J. J. Miret, J. A. Sorni, and S. Vuković, “Propagation of Dyakonon wave-packets at the boundary of metallodielectric lattices,” <https://dx.doi.org/10.1109/JSTQE.2012.2230153> IEEE J. Sel. Top. Quantum Electron. **19**, 4601408 (2013).
- [32] T. G. Mackay and A. Lakhtakia, “Temperature-mediated transition from Dyakonov surface waves to surface-plasmon-polariton waves,” <https://dx.doi.org/10.1109/JPHOT.2016.2611700> IEEE Photon. J. **8**, 4802813 (2016).
- [33] 3M, <https://www.3m.com/3M/en-US/company-us/search/?Ntt=FC-72> Fluorinert™ Electronic Liquid FC-72 (accessed 01 August 2020).
- [34] C. Zhou, T. G. Mackay, and A. Lakhtakia, “Two Dyakonov–Voigt surface waves guided by a biaxial–isotropic dielectric interface,” <https://dx.doi.org/10.1038/s41598-020-69727-z> Sci. Rep. **10**, 12894 (2020).